Available online at www.sciencedirect.com
ScienceDirect
Ocean Engineering 34 (2007) 1532–1542
OCEAN ENGINEERING
www.elsevier.com/locate/oceaneng

Transient behavior of towed cable systems during ship turning maneuvers

Mark A. Grosenbaugh*

Department of Applied Ocean Physics and Engineering, Woods Hole Oceanographic Institution, Woods Hole, MA 02543-1109, USA

Received 19 October 2006; accepted 9 January 2007
Available online 31 January 2007

Abstract

The dynamic behavior of a towed cable system that results from the tow ship changing course from a straight-tow trajectory to one involving steady circular turning at a constant radius is examined. For large-radius ship turns, the vehicle trajectory and vehicle depth assumed, monotonically and exponentially, the large-radius steady-state turning solution of Chapman [Chapman, D.A., 1984. The towed cable behavior during ship turning manoeuvers. Ocean Engineering 11, 327–361]. For small-radius ship turns, the vehicle trajectory initially followed a corkscrew pattern with the vehicle depth oscillating about and eventually decaying to the steady-state turning solution of Chapman (1984). The change between monotonic and oscillatory behavior in the time history of the vehicle depth was well defined and offered an alternate measure to Chapman's (1984) critical radius for the transition point between large-radius and small-radius behavior. For steady circular turning in the presence of current, there was no longer a steady-state turning solution. Instead, the vehicle depth oscillated with amplitude that was a function of the ship-turning radius and the ship speed. The dynamics of a single 360° turn and a 180° U-turn are discussed in terms of the transients of the steady turning maneuver. For a single 360° large-radius ship turn, the behavior was marked by the vehicle dropping to the steady-state turning depth predicted by Chapman (1984) and then rising back to the initial, straight-tow equilibrium depth once the turn was completed. For small ship-turning radius, the vehicle dropped to a depth corresponding to the first trough of the oscillatory time series of the steady turning maneuver before returning to the straight-tow equilibrium depth once the turn was completed. For some ship-turning radii, this resulted in a maximum vehicle depth that was greater than the steady-state turning depth. For a 180° turn and ship-turning radius less than the length of the tow cable, the vehicle never reached the steady-state turning depth.

Keywords: Cable dynamics; Towed systems; Towing maneuvers

1. Introduction

Much of our present-day knowledge about the configuration of an underwater tow cable during ship turning can be attributed to the steady-state analyses of Choo and Casarella (1972) and Chapman (1984). Chapman's study was more comprehensive. He was able to define a critical ship-turning radius, for a given towing speed, above which the cable/vehicle system maintains an equilibrium shape that is nearly equal to the planar configuration associated with a straight-ahead-towing ship trajectory. In this case, the turning radius and velocity of the vehicle are nearly equal to that of the ship (Fig. 1a). Below the critical turning radius, the towing system effectively collapses (Fig. 1b) resulting in a large increase in the vehicle depth and a large decrease in the vehicle turning radius. Chapman also performed some dynamic calculations and showed that, after the turn is completed, the return to the straight-tow equilibrium configuration is exponential with a decay time constant that depends on, among other things, the weight of the vehicle, the cable parameters (i.e. wet weight, length, and drag), and the tow speed.

The purpose of this paper is to extend the work of Chapman (1984) by performing a detailed analysis of the transient behavior that occurs in going from a straight-tow, planar configuration to a three-dimensional steady-state turning configuration. Calculations presented in Chapman

*Tel.: +1 508 289 2607; fax: +1 508 289 2191.
E-mail address: mgrosenbaugh@whoi.edu.

0029-8018/$ - see front matter © 2007 Elsevier Ltd. All rights reserved.
doi:10.1016/j.oceaneng.2007.01.002

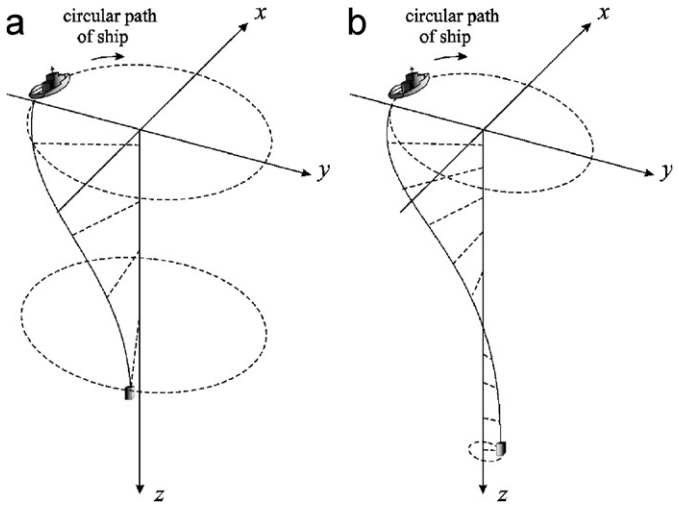

Fig. 1. Turning behavior of a towed vehicle system showing: (a) the near straight-tow configuration that occurs for large-radius or low-speed turns and (b) the non-planar collapse of the tow cable configuration for small-radius or high-speed turns (adapted from Chapman, 1984).

(1984) and the results presented in this paper show that towed vehicle systems rarely reach steady state during typical ship turning maneuvers, especially for small-radius 360° and 180° turns, or in the presence of a current. In these cases, the towing behavior is better described by the transient response. Chapman's stability plots of the collapse of the three-dimensional towing configuration below the critical radius were derived using static analysis. In this paper, we analyze the stability of the towing configuration from a dynamic standpoint and develop an alternate definition for the transition point between large-radius and small-radius turning behavior. We also analyze 360° and 180° turning maneuvers in terms of the transient behavior associated with the change from a straight-tow equilibrium configuration to a steady-state turning configuration.

Our study will be performed using a three-dimensional numerical model of a towed cable system (Gobat and Grosenbaugh, 2000, 2006). While a number of three-dimensional dynamic cable models have been developed in the past to study maneuvering of towed cable systems, none have looked carefully at the open-loop dynamics. Most of the papers on three-dimensional modeling of towed cable systems have concentrated on model development and include only one or two reference problems that highlight the capabilities of the method (Sanders, 1982; Ablow and Schechter, 1983; Delmer et al., 1988; Huang, 1994; Vaz et al., 1997; Buckham et al., 2003; Lambert et al., 2003). A fairly comprehensive study of the 360° turning behavior of towed arrays as a function of turn radius, cable length, and tow speed was performed by Kishore and Ganapathy (1996). They found that during the turning maneuver, a towed array formed a closed loop if the ship-turning radius was less than a specific value that depended on array length and ship speed. This result has similarities with Chapman's critical radius though it did not follow from simulations of steady-state turning maneuvers.

Finally, little is known regarding the behavior of towed cable systems during ship turning maneuvers in currents. Williams (2006) examined open-loop control strategies for ship course and winch motion that would maintain a circular vehicle path at a specified depth. He found that the current caused the control commands to be periodic. We will show, in this paper, that the open-loop response of the vehicle undergoing steady-turning maneuvers in a current is periodic, and that the nature of the periodic response depends on current direction.

2. Methods

The governing equations on which our numerical model is based include the effects of geometric and material nonlinearities and bending and torsional stiffness for seamless modeling of slack cables (Gobat and Grosenbaugh, 2006). The equations are solved using an implicit finite difference scheme that incorporates the generalized-α time integration algorithm, adaptive time stepping, and adaptive spatial gridding to produce accurate, stable solutions for dynamic problems. The nonlinear solver uses adaptive relaxation to improve robustness for both static and dynamic problems. User-specified forcing could include waves, currents, wind, and ship speed. Our computer program has undergone extensive verification including successful comparisons with laboratory data (Gobat et al., 2002) and with results of full-scale experiments of towed and moored systems (Gobat and Grosenbaugh, 1998, 2001).

As a further verification for this study, we performed dynamic simulations of a tow cable system (ship, tow cable, and towed vehicle) going from a straight-tow equilibrium configuration to one in which the tow ship is making a constant radius turn (i.e. steady-state turning configuration). The simulation was allowed to proceed until the towed system reached a steady state with the vehicle making its own constant radius turn and maintaining a constant depth. These results were then compared to those calculated from the steady-state analytical solution of Chapman (1984). The towed system that we used in all the calculations had the following characteristics:

Cable characteristics:

Wet weight per length	$w = 5\,\mathrm{N/m}$
Mass per length	$m = 0.751\,\mathrm{kg/m}$
Added mass per length	$m_a = 0.241\,\mathrm{kg/m}$
Diameter	$d = 0.0173\,\mathrm{m}$
Length	$L = 4000\,\mathrm{m}$
Normal drag coefficient	$C_d = 2.0$
Tangential drag coefficient	$C_t = 0.02$
Axial stiffness	$EA = 4.4 \times 10^9\,\mathrm{N}$
Bending stiffness	$EI = 237.9\,\mathrm{N\,m^2}$
Torsional stiffness	$GJ = 10.0\,\mathrm{N\,m^2}$

Vehicle characteristics:	
Wet weight	$W = 1000\,\mathrm{N}$
Mass	$M = 117.6\,\mathrm{kg}$
Added mass	$M_a = 7.8\,\mathrm{kg}$
Projected frontal area	$A_V = 0.0745\,\mathrm{m}^2$
Drag coefficient	$C_D = 0.0$
Water properties:	
Density of sea water	$\rho = 1025\,\mathrm{kg/m}^3$
Ship input:	
Tow speeds	$V = 0.84,\ 1.19,\ 1.68,\ 2.37,\ 3.75\,\mathrm{m/s}$

The wet weights of the cable and vehicle and the length of the cable are taken from an example given in Chapman (1984). The other cable properties are taken to be consistent with a typical oceanographic tow cable that has a standard diameter of 1.73 cm. The other vehicle properties follow from the assumption that the tow body is cylindrical, but with the vehicle drag coefficient set equal to zero. The zero drag coefficient follows from the assumption built into the analytical solution of Chapman (1984) that the results are for a "heavy fish" where the cable is vertical at the lower attachment point. Using a more realistic vehicle drag coefficient of 1.0 had no effect on the results of these simulations because of the large wet weight and small projected frontal area of the towed vehicle. The non-dimensional scope of the system, defined as $\sigma_o = Lw/W$, is equal to 20.

3. Steady-state turning maneuver

The initial conditions for the simulations in this section consist of the ship towing the cable and vehicle in a straight-tow equilibrium configuration with no ambient current. At time $t = 0$, the ship begins a constant radius turn of radius R (Fig. 2). As the ship begins to turn, the vehicle is pulled on a trajectory that is inside that of the ship's turn. Also, the vehicle sinks to a deeper depth (Fig. 3). As the ship continues turning (making multiple revolutions), the vehicle's turning radius and depth reach steady-state values. For large-radius ship turns, the steady-state turning depth of the vehicle is achieved relatively quickly, and the decrease in the vehicle depth is a small fraction of the original straight-tow equilibrium depth. As the turning radius of the ship decreases, the vehicle's depth overshoots and then oscillates about the final steady-state turning value. The amplitude of the oscillations eventually decays to zero as the vehicle achieves a steady-state turning depth. The overshoot and oscillatory behavior occur when the turn radius R is below a threshold ship-turning radius that depends on the ratio of the wet weight and drag of the cable. The wet weight per unit length of the cable is w and the drag per unit length of the tow cable is defined as

$$r_o = \tfrac{1}{2}\rho V^2\,\mathrm{d}C_d.$$

For $w/r_o = 0.1$ (corresponding to a ship speed of 1.68 m/s), the threshold turn radius between non-oscillatory behavior and oscillatory behavior is about $R_* = 1800\,\mathrm{m}$ (Fig. 3). The threshold radius increases for larger values of w/r_o (e.g. $R_* = 2600\,\mathrm{m}$ for $w/r_o = 0.40$) and decreases for smaller values of w/r_o (e.g. $R_* = 1300\,\mathrm{m}$ for $w/r_o = 0.02$). The threshold turning radius, R_*, is slightly lower than the critical radius defined by Chapman (1984), though it occurs in a range of radii where the vehicle's steady-state turning depth is rapidly changing.

The drop-down ratio for steady turning is defined as

$$\frac{H_{to} - H_o}{L - H_o},$$

where H_o is the straight-tow equilibrium depth and H_{to} is the steady-state turning depth. Fig. 4 shows a plot of the drop-down ratio versus the non-dimensional ship-turning radius (normalized by the length of the cable L) for the same five values of w/r_o used in Chapman (1984). The numerical results were calculated from simulations with ship-turning radii ranging from 0 to 4000 m ($R/L = 0$–1). They are given as solid curves in Fig. 4. Spline interpolation was used in areas where the drop-down ratio was slowly changing and the range increments of the ship-turning radius were larger than 100 m. Drop-down ratio for a select number of ship-turning radii were calculated using Chapman's analytical formula. These results are shown in Fig. 4 as open circles. The match between numerical and analytical results is almost exact.

4. 360° turning maneuver

In this maneuver, the ship completes a single 360° turn of radius R and then returns to a straight course (Fig. 5). Depending on the turning radius of the ship, the towed vehicle will complete a full circular turn with radius nearly equal to that of the ship for a large-radius ship turn, an ellipsoidal loop with a major axis that is much smaller than the diameter of the ship-turning radius for a moderate radius ship turn, or a course deviation with no closed loop for a small-radius ship turn. During the ship turn, the vehicle's depth will increase to a maximum and then rise back to the original straight-tow equilibrium depth (Fig. 6). For large turning radii (in this case for $R > 2400\,\mathrm{m}$ and $w/r_o = 0.1$), the vehicle sinks to its steady-state turning depth before rising back to the steady-state, straight-line depth. For small turning radii (for $R \leqslant 1000\,\mathrm{m}$ and $w/r_o = 0.1$), the vehicle drops to a depth corresponding to the first trough of the oscillatory time series of the steady-state turning maneuver (Fig. 2) before returning to the straight-tow equilibrium depth. The time series results of vehicle depth for other values of w/r_o are similar though the drop-down and recovery processes are compressed in time for smaller values of w/r_o and expanded in time for larger values of w/r_o (Fig. 7).

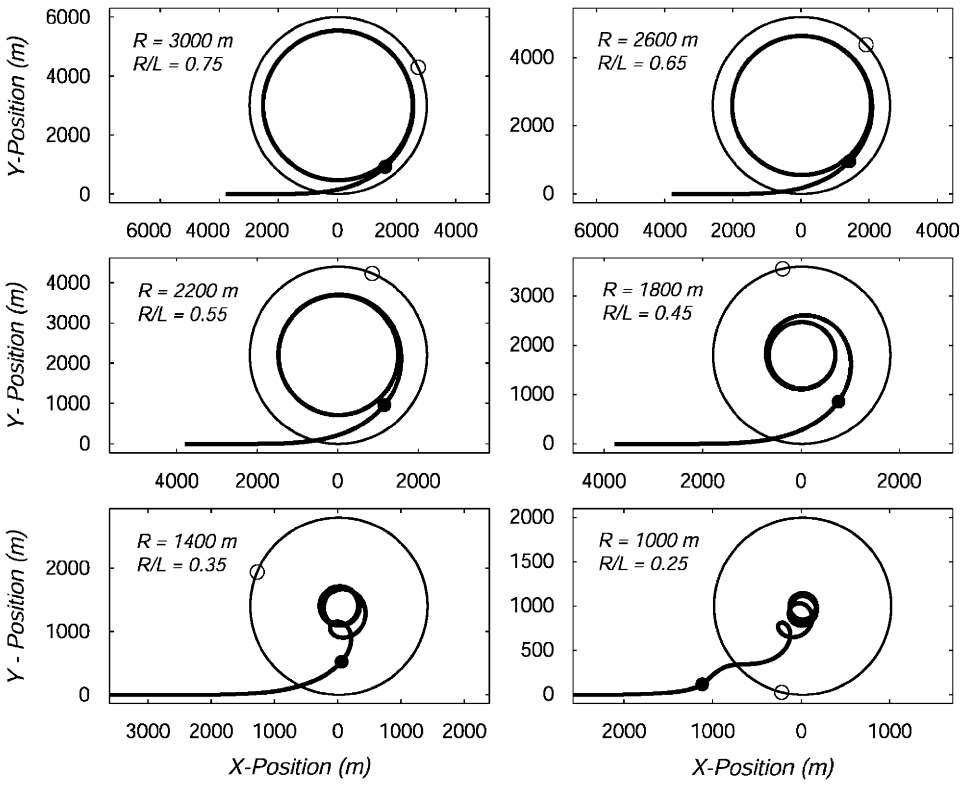

Fig. 2. Horizontal trajectories of ship (thin line) and towed vehicle (thick line) during constant radius, steady-state turning maneuvers for $w/r_o = 0.1$. The symbols represent the position of the ship (open circle) and the vehicle (closed circle) 1 h after the ship begins to turn. The ship and towed vehicle are initially in a straight-tow equilibrium configuration advancing in the positive x-direction. The ship begins its turn at time $t = 0$ and at horizontal position $(x,y) = (0, 0)$.

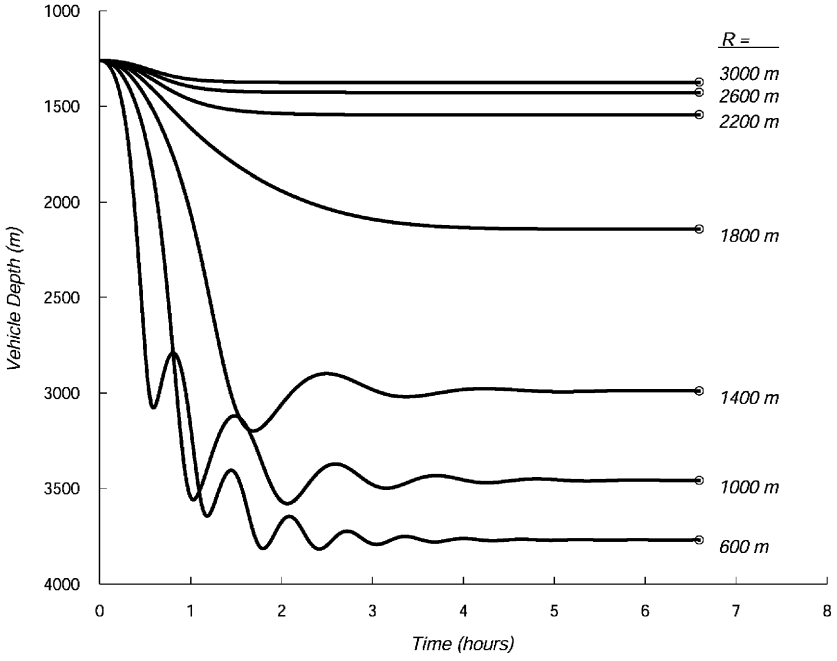

Fig. 3. Time history of vehicle depth during steady-state turning maneuvers as a function of ship-turning radius for $w/r_o = 0.1$.

The maximum drop-down ratio for a particular 360° turning maneuver is defined as

$$\frac{H_{360} - H_o}{L - H_o},$$

where H_{360} is the maximum depth to which the vehicle drops down during the maneuver. This ratio is plotted versus R/L for different values of w/r_o (Fig. 8). The peak in the respective curve gives the largest maximum drop-down ratio for a particular value of w/r_o. The

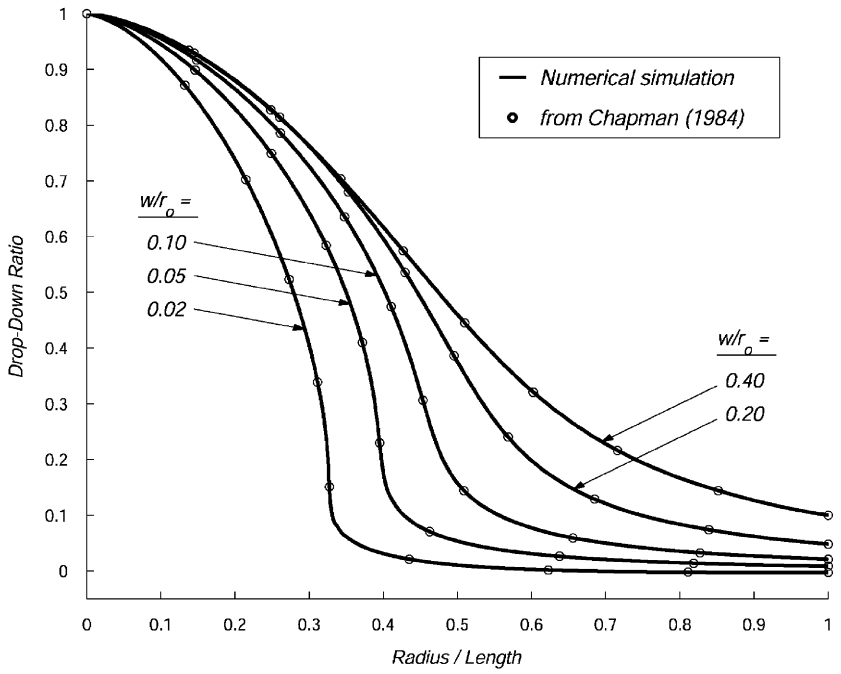

Fig. 4. Drop-down ratio for steady-state turning maneuver plotted versus the radius-to-length ratio for a non-dimensional scope of $\sigma_o = 20$ and different values of w/r_o. The solid lines are results from the numerical simulations. The open circles are based on the steady-state analysis of Chapman (1984).

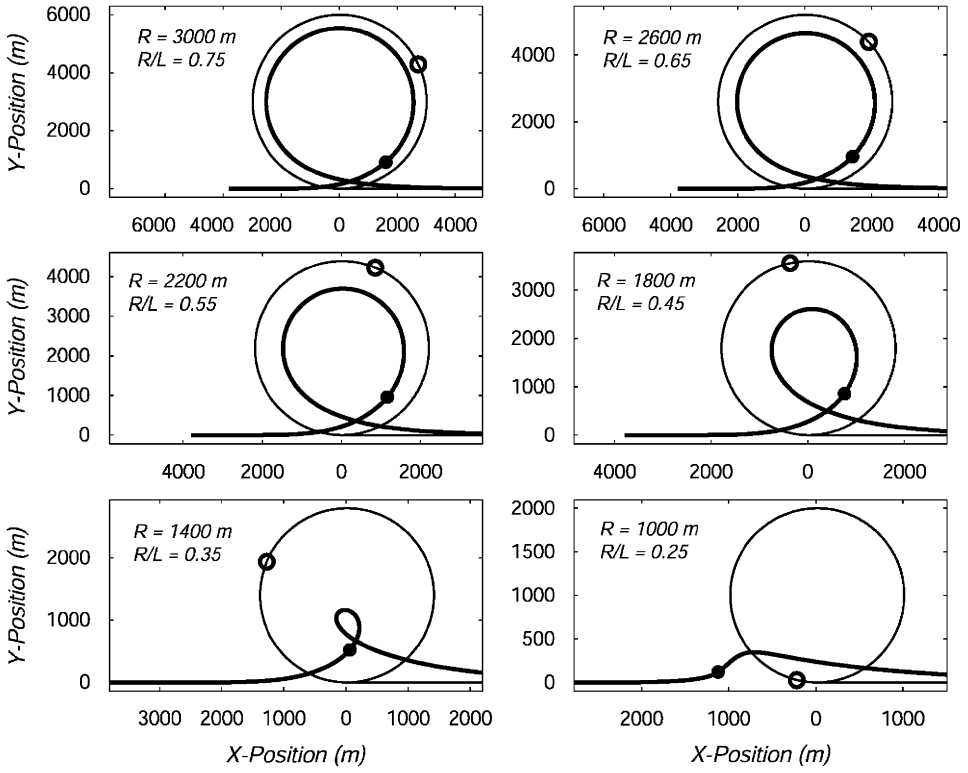

Fig. 5. Horizontal trajectories of ship (thin line) and towed vehicle (thick line) during single 360° turning maneuvers for $w/r_o = 0.1$ (refer to Fig. 2 caption for details).

biggest difference between this maneuver and the steady-state turning maneuver (Fig. 4) occurs as $R/L \to 0$. In the steady-turning maneuver, the towed system essentially has infinite time to collapse into a vertical configuration, which corresponds to a drop-down ratio of 1. For a single 360° turn of zero radius, the turn is instantaneous and the vehicle does not deviate from its straight-tow equilibrium configuration, which corresponds to a maximum drop-down ratio of 0 (Fig. 8).

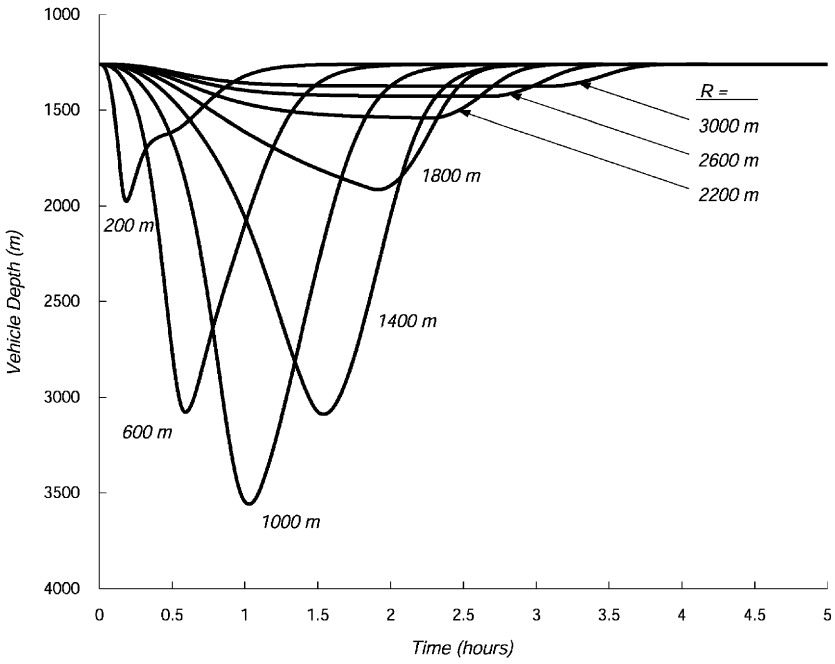

Fig. 6. Time history of vehicle depth during 360° turning maneuvers as a function of ship-turning radius for $w/r_o = 0.1$.

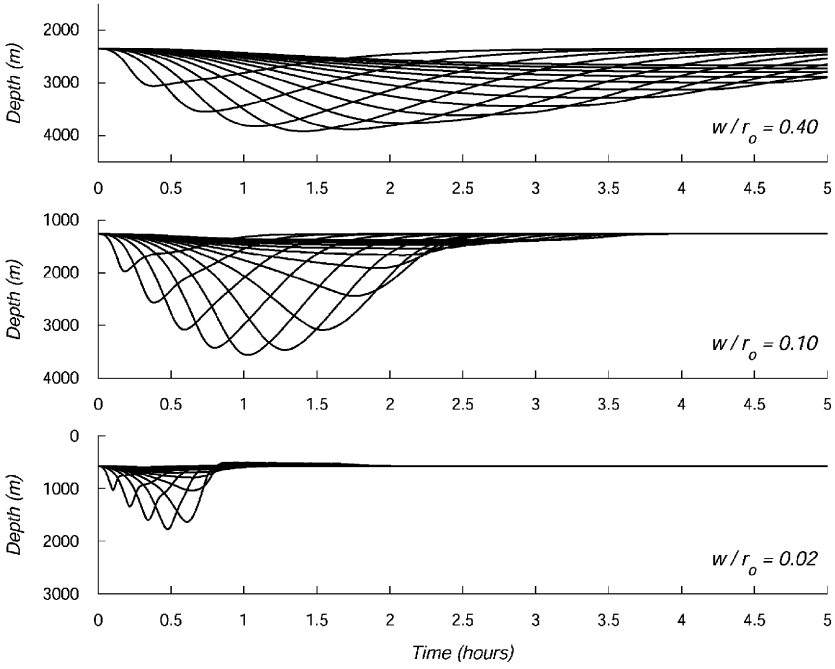

Fig. 7. Time history of vehicle depth during 360° turning maneuvers as a function of ship-turning radius for different values of w/r_o. The contours correspond to ship-turning radii from $R = 200$ m to $R = 3000$ m in increments of 200 m.

5. 180° U-turn maneuver

In this maneuver, the ship performs a 180° turn of radius R and then returns to a straight-tow course but in the reverse direction (Fig. 9). For a large-radius 180° ship turn, the vehicle makes a half-circle turn with a radius that is slightly smaller than the ship-turning radius. The turn center of the vehicle coincides with the turn center of the ship. As the ship-turning radius becomes smaller, the turn center of the vehicle is displaced inward from the turn center of the ship. Also, the vehicle turn develops an asymmetry with the later half of the vehicle turn following a course that moves well inside the ship trajectory. This has the effect of slowing the return of the vehicle to the straight-tow, reversed course of the ship. The return can be speeded-up by initiating the ship turn with a Williamson

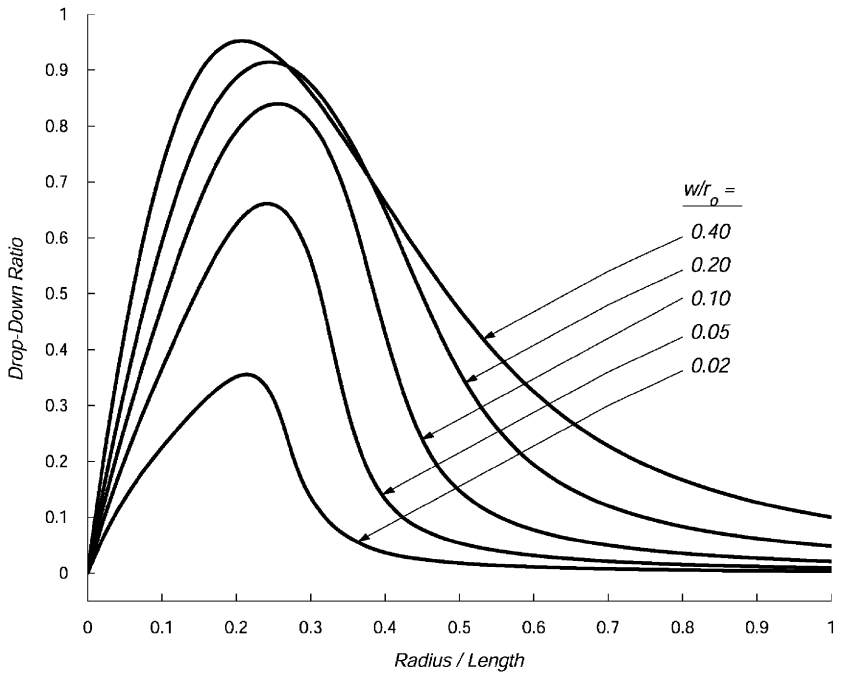

Fig. 8. Maximum drop-down ratio for 360° turning maneuvers plotted versus the radius-to-length ratio for a non-dimensional scope of $\sigma_o = 20$ and different values of w/r.

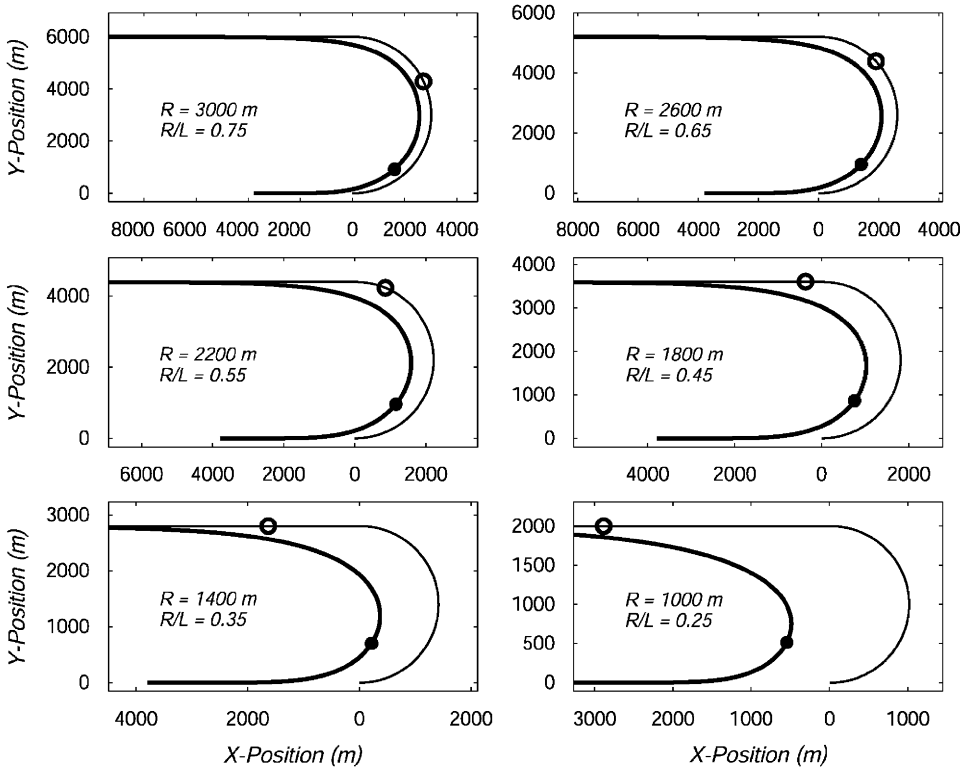

Fig. 9. Horizontal trajectories of ship (thin line) and towed vehicle (thick line) during 180° turning maneuvers for $w/r_o = 0.1$ (refer to Fig. 2 caption for details).

maneuver (Chapman, 1984) or similarly modified 180° ship turn (Lambert et al., 2003).

The time series of vehicle depth for $w/r_o = 0.02$, 0.10, and 0.40 are shown in Fig. 10. In each case, the maximum vehicle depth increases with decreasing ship-turning radius. We define the *maximum drop-down ratio* for a 180° turn as

$$\frac{H_{180} - H_o}{L - H_o},$$

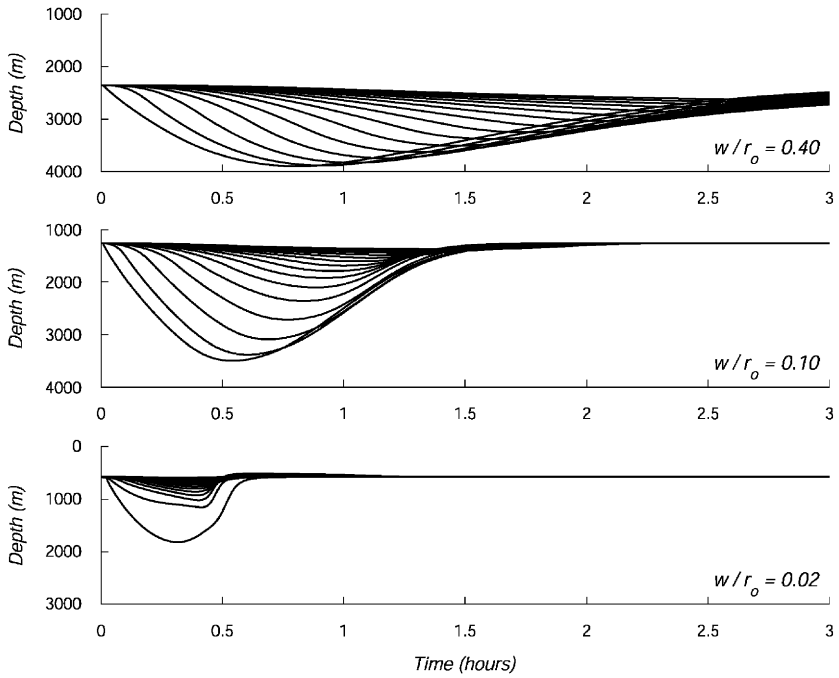

Fig. 10. Time history of vehicle depth during 180° turning maneuvers as a function of ship-turning radius for different values of w/r_o. The contours correspond to ship-turning radii from $R = 0$ m to $R = 3000$ m in increments of 200 m.

where H_{180} is the maximum depth to which the vehicle drops down during the maneuver. The largest maximum drop-down ratio for a particular value of w/r_o occurs for $R/L = 0$, with the maximum drop-down ratio for a given value of R/L increasing with increasing w/r_o (Fig. 11).

6. Transient turning behavior in a current

The analysis of Chapman's (1984) steady-state turning maneuvers described in Section 3 is repeated but with a steady uniform current imposed. Calculations are performed for non-dimensional tow speeds of $w/r_o = 0.02$, 0.10, and 0.40 and with a current that is 20% of the tow speed.

Fig. 12 shows an overhead view of the ship undergoing steady circular maneuvers in the presence of a current. The current, in this case, is parallel to the straight-tow direction (i.e. x-direction). Positive x-current is in the direction of the ship's straight-tow motion and negative x-current is in the reverse direction. Also shown are the resulting vehicle trajectories for the case of $w/r_o = 0.1$ (tow speed of 1.68 m/s and current speed of 0.336 m/s). The thick solid line in each plot corresponds to the vehicle trajectory for the positive-current case and the dashed line corresponds to the negative-current case. As the turning radius of the ship decreases, the area enclosed by the vehicle's turning circle becomes smaller, and the shape becomes more ellipsoidal (e.g. $R = 1800$ m) and eventually irregular (e.g. $R = 1000$ m). The center of the vehicle's turning circle is offset from the center of the ship-turning radius in a direction that is slightly counterclockwise to the direction of the current. The magnitude of the offset is inversely proportional to the ship-turning radius, with the center of the vehicle-turning circle moving outside the ship's turning circle for $R < 1800$ m (for $w/r_o = 0.1$). The angle between the current direction and the offset direction varies with ship-turning radius and is a maximum for $R = 1800$ m (for $w/r_o = 0.1$). Vehicle trajectory results for y-current (current perpendicular to the initial ship track—positive current flows in the direction that the ship is initially turning and negative current opposes the initial turn direction) are similar, except the patterns shown in Fig. 12 are rotated by 90°.

Fig. 13 shows the time history of the vehicle depth during steady-state turning maneuvers in the presence of an x-current. An obvious effect of x-current is to change the starting depth of the vehicle—deeper for positive x-current and shallower for negative x-current. There are also differences in the initial transient behavior due to variations in the current direction, with the biggest differences occurring for small ship-turning radii. Once the transient behavior disappears (for large time), the oscillatory behavior becomes identical for all current directions except for a phase shift that varies with current direction. For large ship-turning radii, the vehicle depth oscillates about the zero-current solution. For small ship-turning radii, the mean of the oscillatory motion is at a shallower depth than steady-state turning depth of zero-current solution.

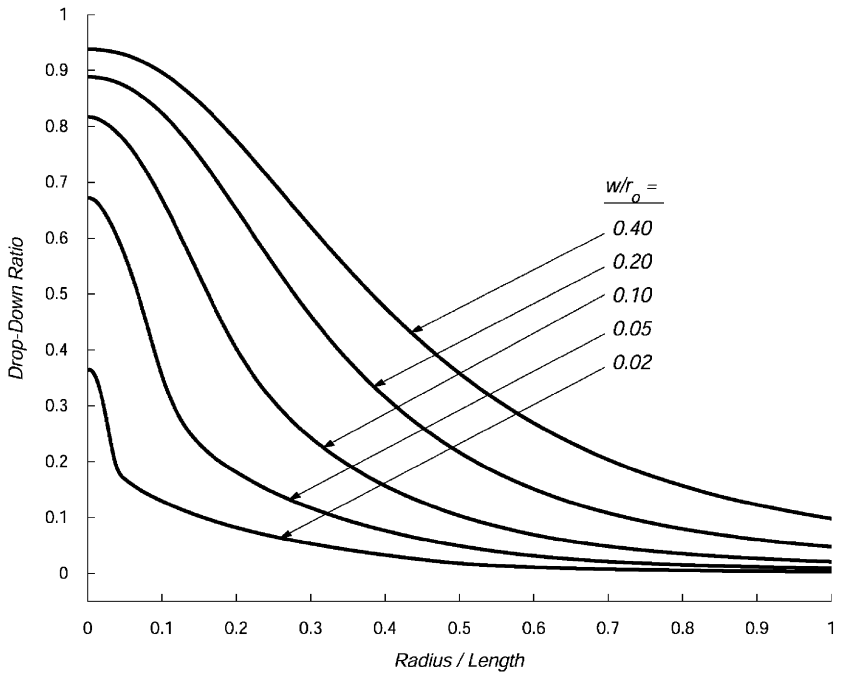

Fig. 11. Maximum drop-down ratio for 180° turning maneuvers plotted versus the radius-to-length ratio for a non-dimensional scope of $\sigma_o = 20$ and different values of w/r.

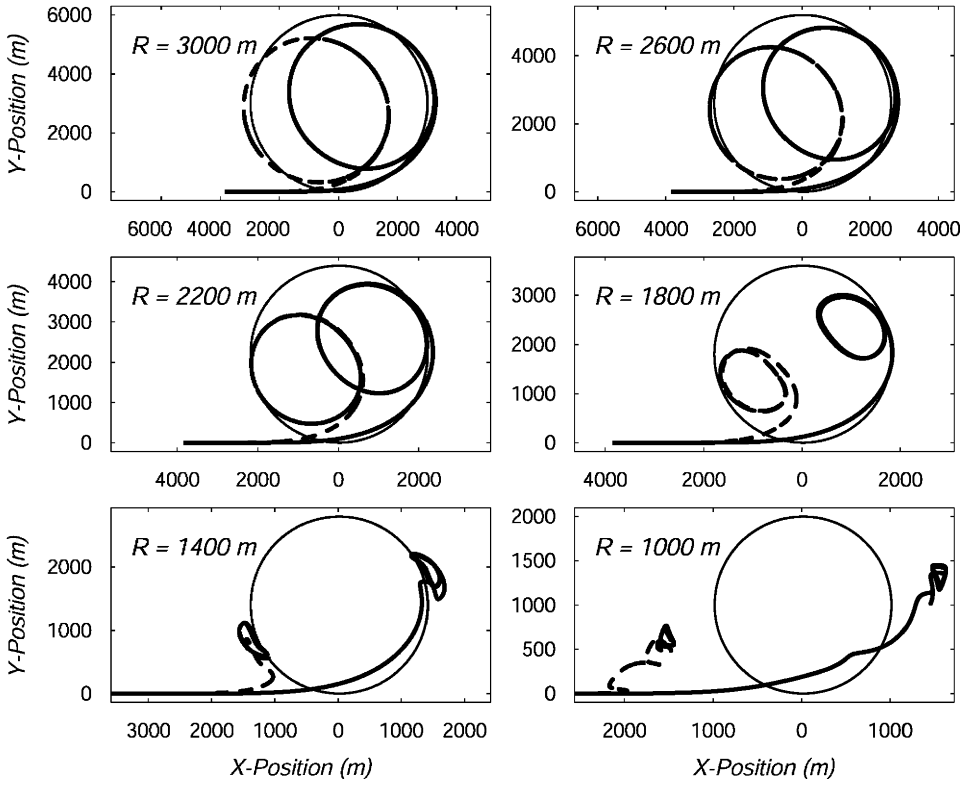

Fig. 12. Horizontal trajectories of ship (thin line) and towed vehicle (thick solid and dashed lines) in a current during constant radius, steady-state turning maneuvers for $w/r_o = 0.1$. The current is 20% of the ship speed. It is in the x-direction and is uniform with depth. Results are shown for positive (solid line) and negative currents (dashed line).

The amplitude of the oscillatory motion is a function of ship-turning radius and ship speed (Fig. 14). It peaks for a ship-turning radius that is slightly below the threshold radius, R_*, defined previously for the no-current case. The oscillatory amplitude dies off as R^{-1} for $R < R_*$ and $R^{-1/2}$ for $R > R_*$.

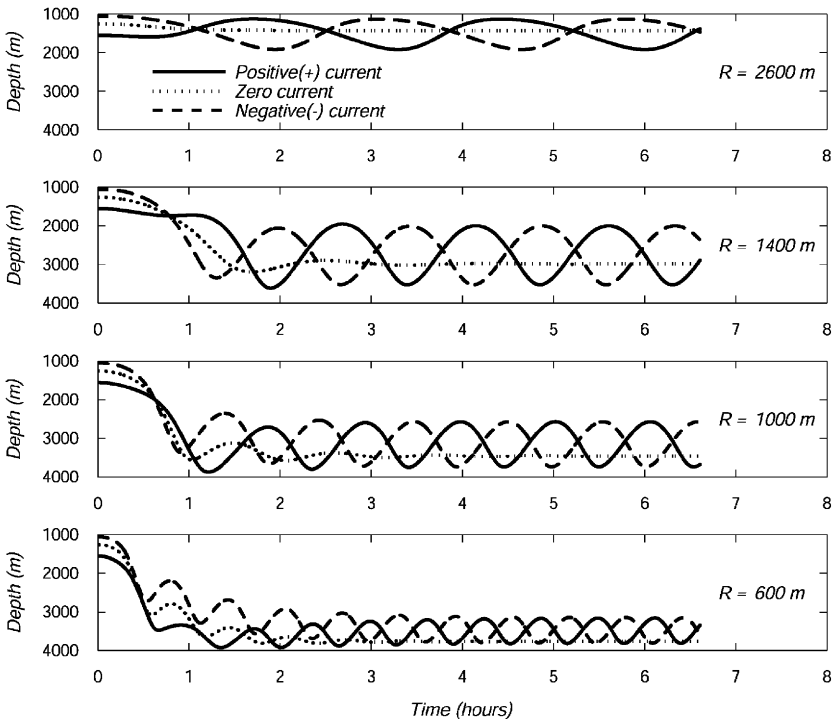

Fig. 13. Time history of vehicle depth during steady-state turning maneuvers in $\pm x$-current for $w/r_o = 0.1$ and selected ship-turning radii. Zero-current results are plotted for reference.

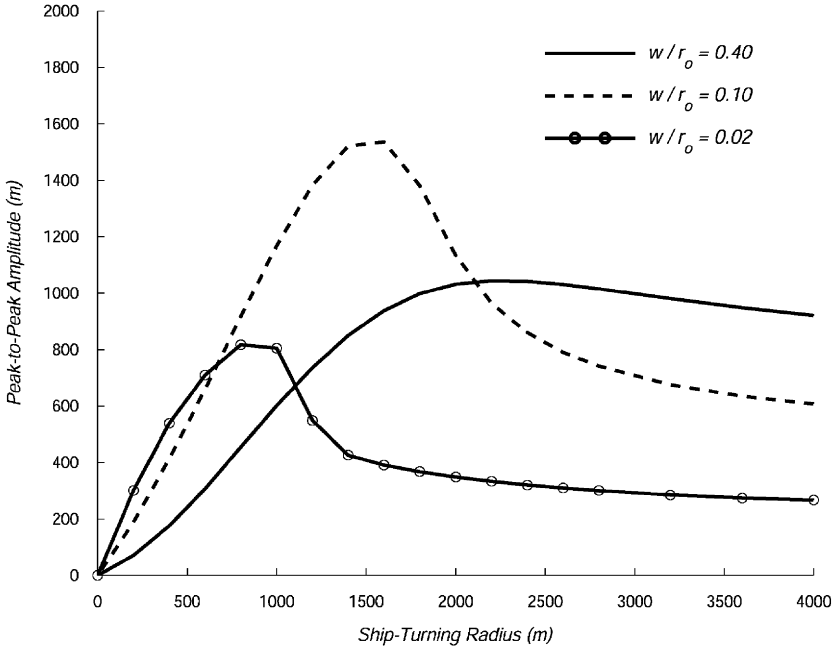

Fig. 14. Asymptotic value of the peak-to-peak amplitude of the vehicle depth for steady-state turning in a current for $w/r_o = 0.02$, 0.10, and 0.40. Non-dimensional scope is $\sigma_o = 20$.

7. Discussion

For large-radius ship turns (without current), the evolution between straight-line configuration and turning configuration is monotonic and exponential. For small-radius ship turns (without current), there is overshoot followed by a decaying oscillation to the steady-state turning configuration (Fig. 3). The overall behavior is analogous to a damped free oscillator. The system displays over-damped characteristics for large-radius turns (no oscillation) and under-damped characteristics for small-radius turns (overshoot and oscillation). The ship-turning radius associated with the change from exponential to oscillatory behavior (defined previously as the threshold

radius R_*), lies within the transition region between the two steady-state configurations identified by Chapman (1984). Introducing currents leads to behavior that is analogous to a forced oscillator. Oscillation is now present in the time history of the vehicle depth for all radius turns. The magnitude of the oscillation varies with ship-turning radius and ship speed. The oscillation amplitude has its largest value for a ship-turning radius that is slightly less than the threshold radius (Fig. 14).

For the 360° turning maneuver, the dynamic behavior is governed by the transient characteristics of the steady-state turning maneuver. The dynamics are a trade-off between the period of the turn and the decay time of the transient. For large-radius, 360° ship turns (i.e. for ship-turning radius much greater than the threshold radius, R_*), the vehicle achieves a steady-state turning configuration in less than one full revolution. As the ship-turning radius decreases the time to complete the turn decreases. Also, as the ship-turning radius approaches the threshold radius, the decay time constant appears to increase (Fig. 3). These factors work together to prevent the vehicle from achieving a steady-state turning configuration in one revolution. Instead, the vehicle follows the initial part of the steady-turning trajectory, but is then pulled back to the straight-tow course before a steady-state turning configuration is reached. For most small-radius ship turns, the maximum depth of the vehicle is less than the steady-state turning depth. However, for some small-radius ship turns, the maximum depth that the vehicle achieves during a 360° turn exceeds the corresponding steady-state turning depth. This occurs if the depth of the initial overshoot of the vehicle is greater than the steady-state depth. The initial overshoot coincides with the completion of the first revolution of the steady-turning maneuver.

The dynamics of the 180° turning maneuver, while still governed by the transient behavior at the beginning of the steady-state turning maneuver, have some major differences with respect to the 360° turning maneuver. The return of the ship to a straight-tow course after a U-turn will cause the vehicle to pull out of its turning maneuver more quickly than for the 360° turn. In fact, the vehicle never reached the steady-state turning depth during the 180° maneuvers for the ship-turning radii used in this study (i.e. $R \leqslant 4000$ m). The other major difference occurred for very small ship-turning radii ($R \leqslant 400$ m) where the maximum depth that the vehicle achieves is greater than for the 360° turn. This is due to time delays in the towing system. When the ship makes a sharp U-turn, the vehicle will continue on its original course for a period of time. The tension in the cable will decrease and the vehicle will sink. The vehicle will continue sinking until the ship has reversed direction and has moved past the vehicle's horizontal x-position. At this point, the ship begins to pull the vehicle in the new direction. For very small 360° ship turns ($R \leqslant 400$ m), the ship completes the maneuver before the vehicle trajectory is considerably altered, and the vehicle quickly resumes the straight-tow equilibrium configuration, since it does not reverse direction. This explains why the vehicle depth and maximum drop-down ratio increases monotonically with decreasing ship-turning radius for the 180° turn (Fig. 11), but not for the 360° turn (Fig. 8).

Acknowledgment

Funding for this work was provided by the Office of Naval Research (Ocean Engineering and Marine Systems) under Grant N00014-04-10030.

References

Ablow, C.M., Schechter, S., 1983. Numerical simulation of undersea cable dynamics. Ocean Engineering 10, 443–457.

Buckham, B., Nahon, M., Seto, M., Zhao, X., Lambert, C., 2003. Dynamics and control of a towed underwater vehicle system, part I: model development. Ocean Engineering 30, 453–470.

Chapman, D.A., 1984. The towed cable behavior during ship turning manoeuvers. Ocean Engineering 11, 327–361.

Choo, Y., Casarella, M.J., 1972. Configuration of a towline attached to a vehicle moving in a circular path. Journal of Hydronautics 6, 51–57.

Delmer, T.N., Stephens, T.C., Tremills, J.A., 1988. Numerical simulation of cable-towed acoustic arrays. Ocean Engineering 15, 511–548.

Gobat, J.I., Grosenbaugh, M.A., 1998. WHOI Cable: time domain numerical simulation of moored and towed oceanographic systems. In: Proceedings of Oceans '98, Nice, France.

Gobat, J.I., Grosenbaugh, M.A., 2000. WHOI Cable v2.0: time domain numerical simulation of moored and towed oceanographic systems. Woods Hole Oceanographic Institution Technical Report. WHOI-2000-08, 89pp.

Gobat, J.I., Grosenbaugh, M.A., 2001. Dynamics in the touchdown region of catenary moorings. International Journal of Offshore and Polar Engineering 11, 273–281.

Gobat, J.I., Grosenbaugh, M.A., 2006. Time domain numerical simulation of ocean cable structures. Ocean Engineering 33, 1373–1400.

Gobat, J.I., Grosenbaugh, M.A., Triantafyllou, M.S., 2002. Generalized-α time integration solutions for hanging chain dynamics. Journal of Engineering Mechanics 128, 677–687.

Huang, S., 1994. Dynamic analysis of three-dimensional marine cables. Ocean Engineering 21, 587–605.

Kishore, S.S., Ganapathy, C., 1996. Analytical investigations on loop-manoeuvre of underwater towed cable-array system. Applied Ocean Research 18, 353–360.

Lambert, C., Nahon, M., Buckham, B., Seto, M., 2003. Dynamics and control of a towed underwater vehicle system, part II: model validation and turn maneuver optimization. Ocean Engineering 30, 471–485.

Sanders, J.V., 1982. A three-dimensional dynamic analysis of a towed system. Ocean Engineering 9, 483–499.

Vaz, M.A., Patel, M.H., Witz, J.A., 1997. Three-dimensional transient behavior of towed marine cables. Journal of Ship Research 41, 45–56.

Williams, P., 2006. Towing and winch control strategy for underwater vehicles in sheared currents. International Journal of Offshore Polar Engineering 16, 218–227.